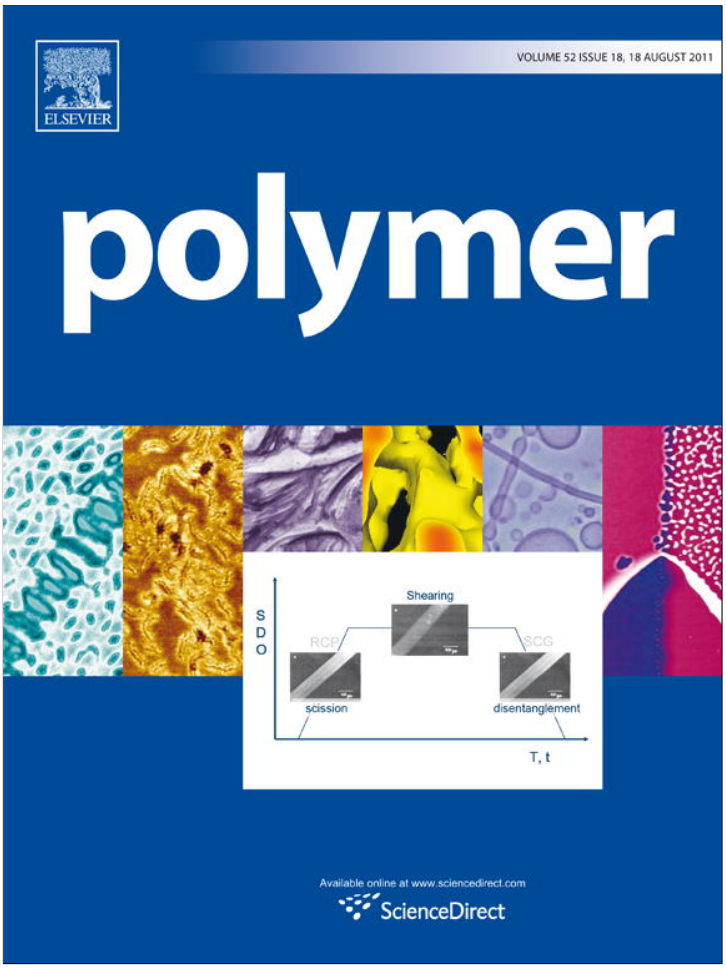

Polymer 52 (2011) 4001–4010

Contents lists available at ScienceDirect

Polymer

journal homepage: www.elsevier.com/locate/polymer

Fabrication of exfoliated graphene-based polypropylene nanocomposites with enhanced mechanical and thermal properties

Pingan Song [a,b], Zhenhu Cao [b,c], Yuanzheng Cai [b,c], Liping Zhao [b,c], Zhengping Fang [b,c,*], Shenyuan Fu [a,**]

[a] Department of Materials, College of Engineering, Zhejiang Agriculture & Forest University, Hangzhou 300311, China
[b] Lab of Polymer Materials and Engineering, Ningbo Institute of Technology, Zhejiang University, Ningbo 315100, China
[c] MOE Key Laboratory of Macromolecular Synthesis and Functionalization, Institute of Polymer Composites, Zhejiang University, Hangzhou 310027, China

ARTICLE INFO

Article history:
Received 12 April 2011
Received in revised form
10 June 2011
Accepted 24 June 2011
Available online 13 July 2011

Keywords:
Graphene
Polypropylene
Mechanical properties, thermal properties

ABSTRACT

Despite the great potential of graphene as the nanofiller, to achieve homogeneous dispersion remains the key challenge for effectively reinforcing the polymer. Here, we report an eco-friendly strategy for fabricating the polymer nanocomposites with well-dispersed graphene sheets in the polymer matrix via first coating graphene using polypropylene (PP) latex and then melt-blending the coated graphene with PP matrix. A ~75% increase in yield strength and a ~74% increase in the Young's modulus of PP are achieved by addition of only 0.42 vol% of graphene due to the effective external load transfer. The glass transition temperature of PP is enhanced by ~2.5 °C by incorporating only 0.041 vol% graphene. The thermal oxidative stability of PP is also remarkably improved with the addition of graphene, for example, compared with neat PP, the initial degradation temperature is enhanced by 26 °C at only 0.42 vol% of graphene loading.

1. Introduction

Compared with traditional composites, polymer nanocomposites exhibit dramatic changes in some properties at very low loadings (generally ≤2 vol%) of nanofillers like exfoliated nano-silicate layers [1–3], carbon nanotubes [4,5], and graphite nanoplatelets [6–9]. However, the performance conferred by these nanofillers can be achieved only when homogeneous dispersion of nanofillers and strong interfacial adhesion between the nanofillers and the polymer matrix are realized. Graphene, a single-layered two-dimensional (2D) structure, is regarded as the strongest material to date by theoretical and experimental results [10,11]. Chemically similar to carbon nanotubes and structurally analogous to silicate layers [12], graphene nanosheets are considered to be the most promising alternative to simultaneously improve the mechanical properties and barrier properties as well as thermal properties. Despite the potential of graphene as the nanofiller, to achieve homogeneous dispersion remains the key challenge for effectively reinforcing the polymer, especially for the non-polar polymer like polypropylene (PP) and polyethylene (PE) [13], two kinds of widely used general plastics in the world. To achieve the uniform dispersion of graphene in the polymer matrix, solution-mixing is the ideal strategy when these polymers can dissolve in common polar organic solvents. To date, it has been successfully achieved to disperse graphene sheets or graphene oxide in some polar polymers such as poly(methyl methacrylate) (PMMA), poly(acrylonitrile) (PAN), poly(acrylic acid) (PAA), polyester, epoxy resin, thermoplastic polyurethane (TPU), poly(vinyl alchol) (PVA) using solution-mixing technique [14–22]. Moreover, exfoliated polystyrene (PS)/graphene nanocomposites are also obtained using phenyl isocyanate-treated graphite oxide and using DMF as the solvent [23].

When it comes to the graphene nanocomposites based on PP and PE, solution-mixing technique becomes impossible since PP and PE are only soluble in solvents like xylene and trichlorobenzene above 120 °C. Galland [24] and Yu [13] have respectively employed the in situ Ziegler–Natta polymerization method to successfully create the exfoliated polyolefin/graphite nanocomposites, however, leaving the mechanical and thermal properties not investigated. Additionally, this method also has limited applicability and scalability. Recently, Song [25] prepared PE/graphene oxide nanocomposites using melt-blending method by adopting PE-grafted-graphene oxide. Despite relative good dispersion of graphene oxide in PE matrix, limited improvements in the mechanical properties were achieved (a maximum increase by ~20% in the

* Corresponding author. MOE Key Laboratory of Macromolecular Synthesis and Functionalization, Institute of Polymer Composites, Zhejiang University, Hangzhou 310027, China. Tel./fax: +86 571 87953712.
** Corresponding author.
E-mail address: zpfang@zju.edu.cn (Z. Fang).

0032-3861/$ – see front matter © 2011 Elsevier Ltd. All rights reserved.
doi:10.1016/j.polymer.2011.06.045

Young's modulus, and ~13% in the tensile strength). Kim et al. [26] have recently also fabricated exfoliated graphene/PE nanocomposites via employing PE functionalized analogs (amine, nitrile and isocyanate) with thermally reduced graphene, and the tensile modulus was greatly enhanced and higher for composites with functionalized PE when 1,2-dichlorobenzene was used as solvent for solvent mixing. Only until recently Torkelson [12,27] successfully prepared the fully exfoliated PP/graphite nanocomposites by the solid-state shear pulverization (SSSP) technique, and incorporating 2.5 wt% graphite could lead to a ~100% increase in the Young's modulus and a ~60% increase in the yield strength relative to neat PP. Moreover, the mechanical performance may still has room to improve at a relatively high loading of 2.5 wt% graphite or remains at a less addition of graphene nanosheets. In addition, latex technology has already been successfully applied for incorporating carbon nanotubes or graphene into a polymer matrix [28–31]. Koning [28,29] uses sodium dodecylsulfate (SDS) or polysaccharide (Gum Arabic, GA) as the surfactant and polystyrene (PS) latex as the polymer matrix to successfully fabricate well-dispersed PS/carbon nanotubes (CNTs) nanocomposites with low percolation thresholds of 0.3 wt%. Miltner [30] has incorporated CNTs into the PP latex with the help of sonication to prepare well-dispersed PP/CNTs composites, and investigated the induced nucleation effect of CNTs on the polymer matrix. Recently, Loos [31] has prepared exfoliated polystyrene (PS)/graphene nanocomposites using poly(styrene sulfonate) (PSS) as the stabilizer for graphene during the reduction of graphene oxide followed by mixing PSS coated graphene with PS latex. All of their work employed the surfactant as the stabilizer of nanofillers and the polymer latex as the polymer matrix.

Here, we report the creation of fully exfoliated PP/graphene nanocomposites with the graphene coated with PP latex, which overcomes the stacking together again of graphene sheets during melt-blending and provides superb polymer–particle interaction and effective load transfer. Consequently, A ~75% increase in yield strength and a ~74% increase in the Young's modulus of PP are obtained by a graphene sheet addition of only 0.42 vol% (1.0 wt%). Compared with Torkelson's work [12,27], comparable improvements in the mechanical properties could be achieved at relatively lower graphene loading. Additionally, the thermal oxidative stability is also significantly improved with the addition of graphene sheets due to the barrier effects. This is very promising to fabricate high-performance polymer nanocomposites with graphene as the nanofiller.

2. Experimental section

2.1. Raw materials

Graphite with an average particle size of 45 μm and a purity of 99.8% were bought from Alfa Aesar Co., Ltd. Sulfuric acid (H_2SO_4), hydrochloric acid (HCl), and hydrogen peroxide (H_2O_2), potassium permanganate ($KMnO_4$), sodium nitrate ($NaNO_3$) were purchased from Sigma–Aldrich and used as received. Hydrazine hydrate (85%) was bought from Changzhou Ruili Chemical Co., Ltd. PP latex was a water-based emulation of maleic anhydride-grafted-isotactic polypropylene (in short PP latex in this study), commercialized by Shanghai Jiaoer Wax Co., Ltd. According to the supplier, the aqueous emulsion is composed of 30 wt% iPP, 5 wt% of anionic surfactant of the oleic acid type, neutralized by an amino-alcohol, the remainder being water. The latex has a solid content of 40 wt%, with a softening point of 150 °C. The weight-average molecular mass (M_w) of the polymer is in the range of 7000–9000 g/mol, and its density is 0.93 g/cm^3. Polypropylene (PP) is a copolymer of propylene (90% by mole ratio) and ethylene (10% by mole ratio) with M_w and M_n of 300 000 and 63 000, respectively. Its melt flow rate is 3.0 g/10 min according to the ASTM D-1238, the density is 0.90 g/cm^3.

2.2. Fabrication of graphite oxide (GO)

The GO was prepared from graphite by the modified Hummers methods [32]. A typical procedure was as follows. Graphite (5 g) was added into a 500 ml flask with 60 ml concentrated H_2SO_4 and 32 g $NaNO_3$. After stirring for 30 min, $KMnO_4$ (15 g) was slowly added into the flask with stirring and cooling by placing the flask into an ice bath to keep the temperature below 20 °C. After oxidizing for 4 h, the mixture was poured into a 1 l beaker, and the reaction was terminated by adding 200 ml distilled water, followed by adding 50 ml H_2O_2 to reduce the excess unreacted $KMnO_4$. The mixture was filtered with distilled water and subsequently 5% HCl aqueous solution until the sulfate could not be detected by $BaCl_2$. The resulting GO was then dried at 25 °C for one week.

2.3. Fabrication of PP-coated graphene

To determine the yield of graphite oxide after reduction, 100 mg of GO was first dispersed in a 500 ml flask with 200 ml distilled water, and exfoliated by sonication for 30 min, then the solution was heated to 98 °C followed by dropping 0.5 ml hydrazine hydrate. After reduction for 6 h, the mixture was filtered under vacuum with a PTFE filter (5 μm pore size), and dried at 80 °C for 12 h to yield a solid black material with a net mass of 60 mg. According to the reduction reaction, a ~60% yield was obtained.

To enable the reduced graphene not to stack or aggregate together again, 100 mg of GO was first dispersed into a 200 ml distilled water, and 0.3 g PP latex was subsequently added to keep the mass ratio of PP latex/graphene at 2/1. When the ratio was lower than 2:1, the black graphene will extremely easily aggregate upon reduction with hydrazine hydrate. Reduction procedure was the same to those above-mentioned, the reduced PP latex–-graphene solution was directly dried up to constant weight at 80 °C instead of filtrating it. ~1.59 g of PP-coated graphene was obtained nearly without any mass loss.

2.4. Fabrication of PP/graphene nanocomposites

Depending on the wt% of graphene, the detailed formulations are listed in Table 1. Since graphene tended to restack to layered structure after filtration, it was very difficult to prepare well-dispersed PP/graphene nanocomposite through melt-blending technique, while the graphene coated by PP latex (for short PP-coated graphene) could be readily blended with PP matrix. The PP-coated graphene and PP were pre-compounded manually and then were melt blending using a MiniLab Haaker mixer with a rotation speed of 150 rpm at 180 °C for 10 min. The composites were hot-pressed at 180 °C under 10 MPa into sheets with a thickness of 1 mm.

Table 1
The formulation of PP/graphene nanocomposites and corresponding sample identification. The volume fraction (vol%) is calculated according to their mass fractions and densities.

Sample ID	PP (wt%)	PP latex (wt%)	Graphene (wt%)	Graphene (vol%)	T_p[a] (°C)	χ_c[a] (%)	σ_c (S m^{-1})
Neat PP	100	0	0	0	116.0	42.0	3.2×10^{-13}
PPG-0.1	99.7	0.2	0.1	0.041	117.5	41.6	1.3×10^{-12}
PPG-0.5	98.5	1.0	0.5	0.21	117.7	42.8	3.6×10^{-10}
PPG-1.0	97.0	2.0	1.0	0.42	117.9	42.7	2.7×10^{-9}
PPG-2.0	94.0	4.0	2.0	0.83	118.5	43.1	4.5×10^{-5}
PPG-5.0	85.0	10.0	5.0	2.1	120.3	44.7	1.8×10^{-4}

[a] T_p: peak temperature of non-isothermal crystallization, χ_c: crystallinity, σ_c: electrical conductivity.

Table 2
Mechanical properties of PP/graphene nanocomposites with various graphene loadings.

Sample ID	YS[a] (MPa)	TS[a] (MPa)	YS[a]↑	YM[a] (GPa)	YM[a]↑	EB[a] (%)
Neat PP	22 ± 0.8	24 ± 0.8	–	1.02 ± 0.10	–	1120 ± 100
PPG-0.1	30 ± 1.1	33 ± 1.4	36%	1.25 ± 0.12	23%	1150 ± 120
PPG-0.5	36 ± 1.2	36 ± 1.5	50%	1.50 ± 0.15	47%	330 ± 30
PPG-1.0	38 ± 1.7	37 ± 1.6	75%	1.76 ± 0.25	74%	130 ± 20
PPG-2.0	33 ± 1.4	32 ± 1.0	51%	1.66 ± 0.20	63%	120 ± 18
PPG-5.0	27 ± 0.8	27 ± 0.8	13%	1.23 ± 0.13	21%	100 ± 15

[a] YS, TS, YS↑, YM, YM↑, and EB refer to the yield strength, tensile strength, percent increment of yield strength, Young's modulus, percent increment of Young's modulus, and elongation at break, respectively. The values following ± are errors of one standard deviation.

To investigate the potential effects of PP latex on the nanocomposites, the PP/PP latex blends with various PP latex loadings were also fabricated with the same fabrication methods to the PP/graphene nanocomposites mentioned above. As for the sample identification, e.g. 0.2 wt% PPl means that PP/PP latex blend contains 0.2 wt% PP latex.

2.5. Characterization

Typical tapping-mode atomic force microscopy (AFM) measurements were carried out using Multimode SPM from Digital Instruments with a Nanoscope IV controller made by Veeco Instruments Inc. The sample for AFM tests was fabricated by depositing an aqueous solution of graphite oxide (1.0 mg/ml) onto a fresh mica surface and allowing them to dry in air at room temperature. Transmission electron microscopy (TEM) images were obtained using a JEM-1230 instrument at an acceleration voltage of 120 kV. For the TEM observations of GO and PP-coated graphene, their samples were prepared by dispersing them into distilled water to form corresponding aqueous solution (1.0 mg/ml), and for PP/graphene composite, its sample for TEM observation was obtained by freezing ultrathinned sectioning with a thickness of ~80 nm. The micro-morphology of the cross-section and profile of sample after tensile tests were observed using a field emission scanning electron microscope (FEI-SEM S4800) at an acceleration voltage of 5.0 kV. Raman spectra of various samples were carried out with an ALMEGA-Dispersive Raman (Thermo Nicolet) with 514.5 nm excitation. X-ray diffraction (XRD) was carried out using a Rigaku X-ray generator (Cu Kα radiation with $\lambda = 1.54$ Å) at room temperature. Tensile measurements were performed using a WD-5 Electronic Tensile Tester at an extension rate of 10 mm/min at 25 ± 2 °C, and the data reported in Table 2 were the means of quintuplicate measurements. For neat PP, PPG-0.1 and PPG-0.5 sample, the electrical conductivity (σ_c) was measured with a ZC36F ultrahigh resistance (Shanghai Taiou Electric Co. Ltd, China). In the case of PPG-1.0, PPG-2.0 and PPG-5.0, their σ_cs were determined using a RTS-4 four-probe multimeter (Guangzhou 4 Probes Tech Co. Ltd, China) at room temperature. The thermal conductivity κ was calculated by using $\kappa = D\rho_d C_P$, where D, ρ_d, and C_P are the density, thermal diffusivity, and specific heat of samples, respectively, which were measured by a laser flash method on a Netzsch LFA457 with a Pyroceram standard at room temperature.

Tensile properties of samples were performed on a WD-5 Electronic Tensile Tester (all samples were measured in quintuplicate). Dynamic mechanical analysis (DMA) was conducted using a dynamic mechanical analyzer (DMA242C, TA) at a frequency of 1 Hz with a heating rate of 3 °C/min from −50 °C to 150 °C. The glass transition temperature (T_g) was determined from the peak of loss factor (tan δ)—temperature plots. Thermogravimetric analysis (TGA) was performed on a TA SDTQ600 thermal analyzer at a scanning rate of 20 °C/min in air with a temperature range of 50–600 °C. The TGA tests were done in triplicate for each sample. The reproducibilities of temperature were ±1 °C. Differential scanning calorimeter (DSC) was used for investigating the crystallization using a non-isothermal 10 °C/min cooling ramp.

3. Results and discussion

3.1. Fabrication and characterization of PP/graphene nanocomposites

To fabricate well-dispersed PP/graphene nanocomposites, a strategy by combination of pre-solution-mixing and subsequent melt-blending is employed, and the schematic representation of fabricating the nanocomposites is presented in Scheme 1. Graphite oxide (GO) was first prepared via the modified Hummers methods [32] as described elsewhere. A certain amount of dry GO was then dispersed and exfoliated into individual sheets in an aqueous solution of stoichiometrical PP latex by intermittent ultrasonication for 30 min. After the solution was heated up to 98 °C, an amount of hydrazine hydrate was dropped to reduce the GO, and the PP latex could simultaneously absorb onto the reduced graphene sheets to prevent them from stacking or aggregating again. Upon completion of the reduction reaction, the solution was dried and the PP-coated graphene was obtained. The PP-coated graphene was subsequently melt blended with PP matrix to fabricate the PP/graphene nanocomposites.

Atomic force microscopic (AFM) image, as shown in Fig. 1A, reveals that most individual graphite sheets has an average height of about 0.75 nm, indicating the characteristic of a completely exfoliated graphene sheet [23,33,34], with about 1.0 μm in length and around 0.7 μm in width. TEM images (Fig. 1B) also show that graphene was completely exfoliated into wrinkled single sheets by ultrasonic treatment, and its size agrees well with the AFM

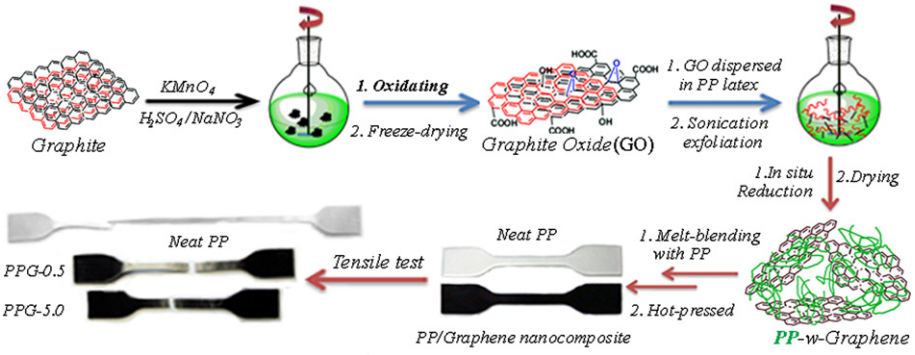

Scheme 1. Schematic representation of process flow of polypropylene (PP)/graphene nanocomposites fabrication and the tensile tests.

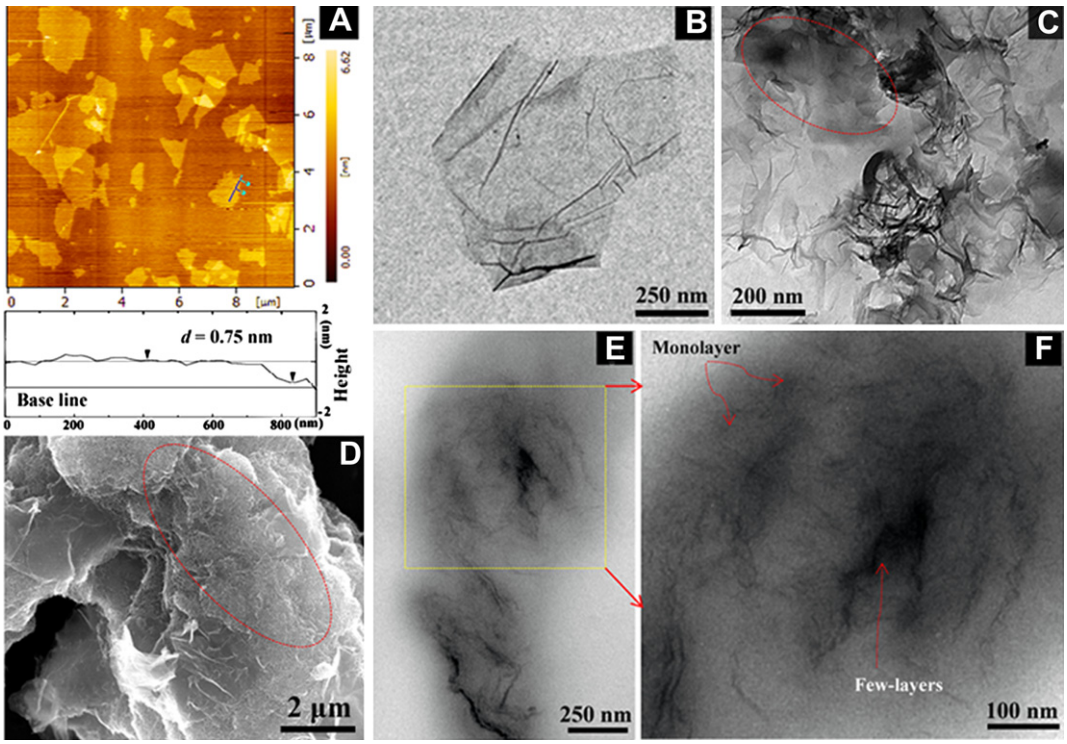

Fig. 1. Micrographs of (A) a typical AFM image and (B) a TEM image of graphene sheets deposited onto a mica substrate from an aqueous dispersion, (C) Typical TEM, (D) Typical SEM images of PP-coated graphene, the PP latex was marked by the red circles, and (E, F) dispersion of graphene in PP matrix.

observations. After coated with PP latex, TEM and SEM images (Fig. 1C, D) clearly display that the surface of the reduced graphene was coated with a polymer film (marked by red circles). To verify the polymer film was the PP latex, energy dispersive X-ray microanalysis (EDAX) was conducted and the results show that PP-coated graphene is composed of 82.2 wt% C, 13.5 wt% O, 2.1 wt% Na and 2.2 wt% K, while 80.4 wt% C and 19.6 wt% O for the graphene reduced under the same condition. Thus, the K and Na elements primarily come from the PP latex, implying the graphene was coated by the PP latex.

Since hydrazine primarily reduces both epoxy and hydroxyl groups in graphene oxide [33], the remaining unreduced carboxyl groups will still have strong interaction like H-bonding with the carboxyl groups in PP latex macromolecules. Therefore, PP latex can readily coat the reduced graphene and the PP-coated graphene was expected to have good compatibility with the PP matrix for the chemical structure of PP latex is essentially identical to PP matrix. TEM images (Fig. 1E, F) of PP nanocomposite containing 1.0 wt% graphene verify that the majority of graphene are basically fully exfoliated into single sheets with bits of few-layers (marked by red arrow).

The electrical conductivity can be generally used to determine the dispersion of conductive fillers in the polymer matrix [12,13,35,36]. The electrical conductivity (σ_c) of PP and its graphene nanocomposites are given in Table 1. Neat PP displays virtually zero conductivity of 3.2×10^{-13} S m^{-1}. The conductivity of PP composites increases with increasing graphene loading and exhibits a relatively high conductivity of $\sim 10^{-5}$ S m^{-1} only when the loading of graphene reaches 2.0 wt%, implying the formation of conductive network through the polymer matrix. Namely, the percolation threshold of conductivity is between 1.0 wt% and 2.0 wt % graphene loading, which is very close to the reported values [12,13]. On the other hand, the results also demonstrate that graphene is well exfoliated in the PP matrix, since this low percolation threshold only can be achieved when graphene nanoplatelets are well-dispersed.

Raman spectroscopy is employed to evaluate the hybridization of state in carbon [37,38], and the two reflections peak changes from pristine graphite to its derivatives. As shown in Fig. 2, a strong band at 1580 cm^{-1} (G band) and a relatively weak band at 1352 cm^{-1} (D band) appear in the Raman spectra of pristine graphite, which stem from the vibration of sp^2-hybridized graphitic domains [37], and sp^3-hybridized carbon or structural defects [39], respectively. The low I_D/I_G value (0.20) indicating the graphitic domains is primarily intact for pristine graphite. After oxidation, both bands are broadened and shifted to slightly higher wavenumber accompanied by significant increase in I_D/I_G value (1.01). Generally, the increase in I_D/I_G value reflects the increase in the defect-like amorphous domains [38], thus the enhanced I_D/I_G value for GO is attributed to the isolation of carbon double bonds due to

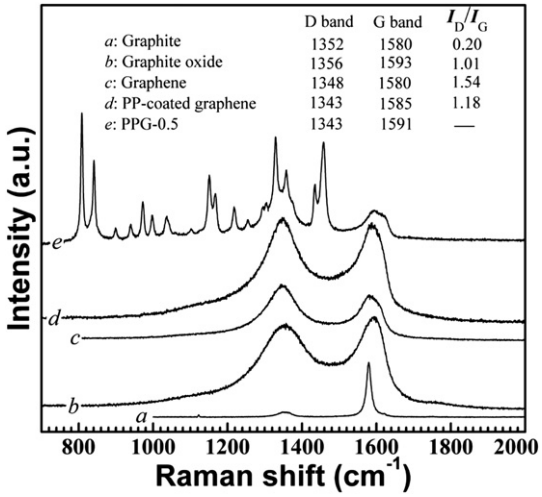

Fig. 2. Raman spectra of (a) pristine graphite, (b) graphite oxide, (c) graphene, (d) PP-coated graphene, and (e) PP nanocomposite with 0.5 wt% graphene (PPG-0.5).

oxidation. As expected, the peak locations of both bands almost return to the same locations to pristine graphite after reduction. Both bands, however, remain much broader than those of pristine graphite and I_D/I_G value increases relative to that of GO, which is also observed by several studies [22,32,40] and they attributed this change to the increase in the number of aromatic domains of smaller overall size in reduced graphene [32] or highly defected carbon lattice after chemical reduction [40]. For PP-coated graphene, the location of the two peaks changes slightly, and the I_D/I_G value reduces to some extent in the presence of PP latex. These changes indicate that the presence of PP latex to certain extent affects slightly the effectiveness of reduction according to the explanation of Paredes et al. [40].

X-ray diffraction (XRD) allows us to detect the interlayer distance between graphite sheets and the exfoliation state of graphene. As shown in Fig. 3A, for pristine graphite, a strong sharp reflection at $2\theta = 26.5^\circ$, corresponding to an interlayer spacing of 0.34 nm. After oxidation, the interlayer spacing is increased up to 0.80 nm due to the intercalation by oxygen containing groups or absorbed moisture [37]. A broad diffraction peak appears centered at 21.4°, giving an interlayer distance of 0.42 nm for the graphene reduced by hydrazine hydrate, indicating that the graphene nanosheet stacks again due to the strong Van der Waals' forces in the interlayer. Almost no diffraction peak is observed in the XRD patterns of dry PP latex and PP-coated graphene, inferring that PP latex is totally amorphous and cannot crystallize, and the complete exfoliation of graphene without stacking together again due to the presence of PP latex. For PP/graphene nanocomposites with various graphene loadings, no diffraction peaks are observed except the crystalline diffraction peaks of the PP matrix (Fig. 3B), indicating that graphene is basically exfoliated into individual sheets and well-dispersed in PP matrix. It is readily observed that the presence of graphene sheets affects the crystallization behaviors of the matrix to some extent from the changes of the {(110), (040), (130)} crystal face [41–43]. To investigate the effects of graphene on the crystallization dynamics of PP, DSC tests were carried out. As shown in Fig. 4, compared with neat PP, the non-isothermal crystallization peak temperature (T_p) gradually increases with increasing graphene loading level, which demonstrates that the graphene nanoplatelets can act as seeds for faster nucleation (see Table 1). However, Torkelson et al. [27] observed that the presence of graphite resulted in a wider and shallower exothermic curves, while in our PP/graphene systems the presence of graphene seems not to affect the shape of exothermic curves; this is likely due to the difference in the kind of PP resin, the fillers (graphite and graphene), and the fabrication method. The crystallinity of PP and its nanocomposites can be calculated by DSC (the enthalpy of 100% crystallinity of PP is 109 J/g [44]). An increase in graphene leads to an increase in the crystallinity of PP, indicating that the graphene can also act as seeds to induce the crystallization of PP.

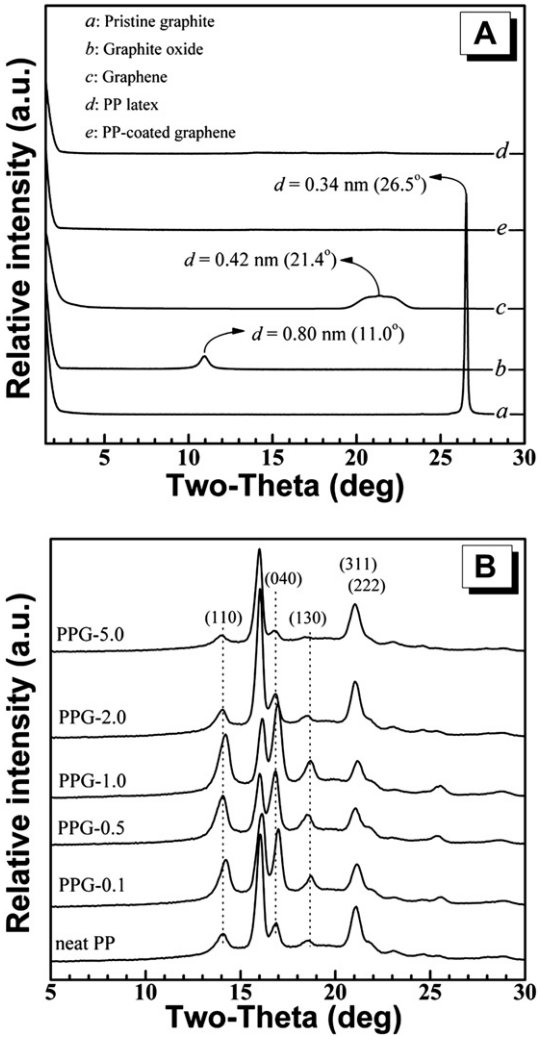

Fig. 3. XRD patterns (A) of (a) pristine graphite, (b) graphite oxide, (c) graphene, (d) PP latex, and (e) PP-coated graphene; (B) PP/graphene nanocomposites with various graphene loadings.

3.2. Mechanical properties of PP/graphene nanocomposites

Since TEM observations and XRD results reveal that graphene sheets are basically fully exfoliated in the presence of PP latex, a considerable enhancement in the mechanical performance of PP matrix will be expected by incorporating the graphene sheets with large aspect ratio. Fig. 5A presents the typical stress–strain plots of PP/graphene nanocomposites as a function of graphene loading, with the detailed data listed in Table 2. Clearly, incorporation of graphene nanosheets results in a significant enhancement in the mechanical strength and Young's modulus at low graphene loading, herein, not exceeding 1.0 wt%. Simultaneously, the elongation at break of the nanocomposites reduces with increasing graphene loading level. Upon incorporating 0.1 wt% graphene, the yield strength, tensile strength and Young's modulus are increased up to 30 MPa (by 36%), 33 MPa (by 38%), and 1.25 GPa (by 23%),

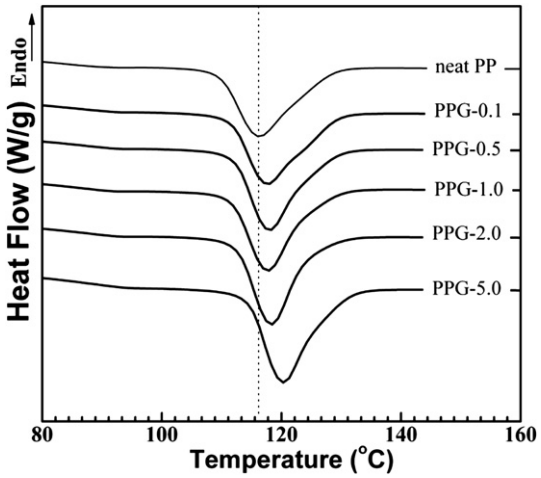

Fig. 4. Non-isothermal (10 °C/min) curves for neat PP and PP/graphene nanocomposites.

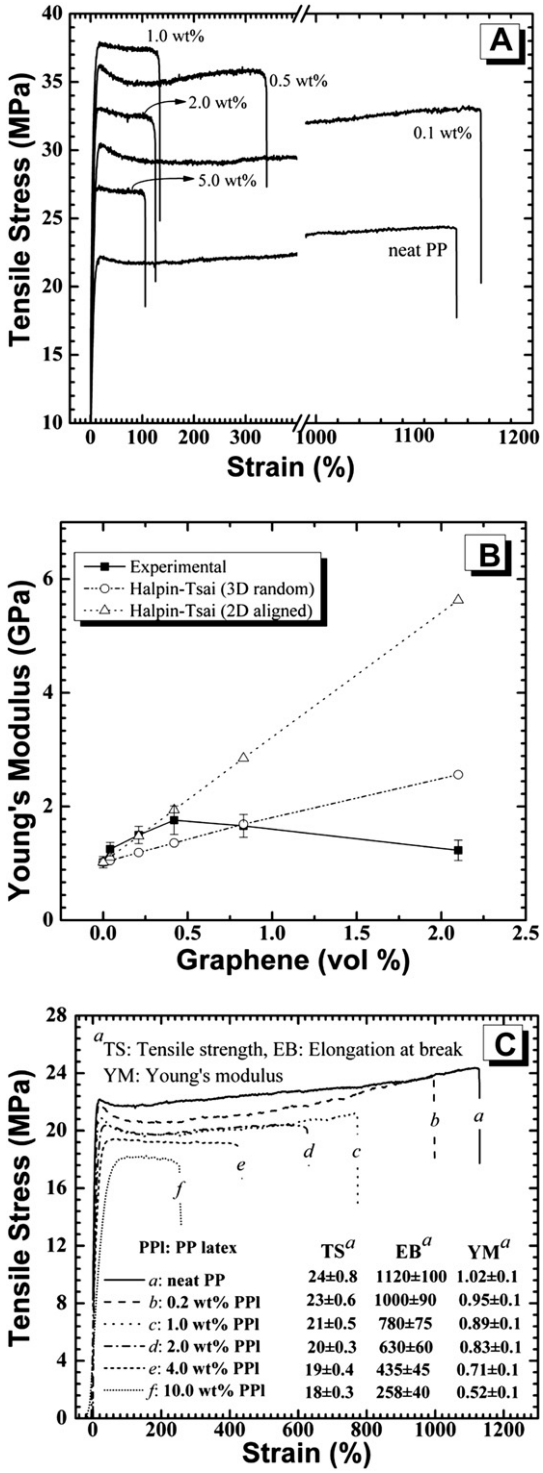

Fig. 5. (A) Representative stress–strain behavior of PP/graphene nanocomposites with various graphene loadings. With only 1.0 wt% graphene, the yield stress and tensile stress of the composite increased by 73% and 54% relative to the parent polymer, respectively. (B) Experimental Young's modulus of the nanocomposites, calculated results obtained from the Halpin–Tsai model under the hypothesis that graphene sheets randomly dispersed as 3D network, and graphene aligned parallel (2D) to the surface of the nanocomposites. (C) Typical stress–strain curves of PP/PP latex as a function of PP latex loading level with detailed data presented in the figure.

respectively. Furthermore, the elongation at break is nearly unchanged, indicating no reduction in the toughness of the nanocomposite. As the graphene loading reaches 1.0 wt%, all mechanical strengths and modulus also reach the maximum values. The yield strength (38 MPa), tensile strength (37 MPa), and Young's modulus (1.76 GPa) are enhanced by 75%, 54%, and 74%, respectively. While Torkelson recently observed that addition of up to 2.5 wt% graphite leads to an about 60% increase in yield strength and a 100% increase in Young's modulus relative to neat PP by using solid-state shear pulverization (SSSP) technique at loading [12]. These enhancements are attributed to the homogeneous dispersion of graphene nanosheets and effective load transfer from the matrix to graphene due to their strong interfacial adhesion. However, with further increase in graphene loading above 2.0 wt% in this study (see Table 2), all mechanical indexes reduce gradually. Zhang et al. [22], in their PVA/graphene nanocomposites, considered that there is a critical point of the mechanical properties or "mechanical percolation" similar to electrical or rheological percolations [45]. Namely, lower than this point, the graphene sheets can be fully exfoliated in the polymer matrix and effective reinforcement can be achieved, while further loading will cause the stacking together again of graphene nanosheets due to the strong van der Waals' force between the nanosheets. While in our experiments, the critical point of so-called "mechanical percolation" seems not to take place since no new diffraction peaks appear in the XRD results of both PPG-2.0 and PPG-5.0. Thus, the phenomenon is more likely attributed to the plasticization effect on the mechanical properties caused by the presence of low molecular PP latex (interfacial compatibilizer) due to its very lower mechanical strength and modulus in comparison with the host PP matrix. If the magnitude of enhancement in the mechanical properties conferred by incorporating graphene cannot compensate for that of reduction in the mechanical properties due to the presence of PP latex, the mechanical performance will decrease with increasing graphene loading since the amount of PP latex also simultaneously increases.

Halpin–Tsai equation is widely used to approximately predict the modulus of unidirectional or randomly dispersed filler-reinforced composites [21,22,46,47]. For randomly oriented or unidirectional graphene sheets in the polymer matrix, the Young's modulus of the nanocomposite with randomly distributed graphene sheets (E_c) and the Young's modulus of the nanocomposite with graphene sheets aligned parallel to the surface of the sample film (E_{paral}) are given as follows:

$$E_C = E_m\left[\frac{3}{8}\frac{1+\xi\eta_l\nu_g}{1-\eta_l\nu_g}+\frac{5}{8}\frac{1+2\eta_t\nu_g}{1-\eta_t\nu_g}\right] \quad (1)$$

$$E_{Paral} = E_m\left[\frac{1+\xi\eta_l\nu_g}{1-\eta_l\nu_g}\right] \quad (2)$$

$$\eta_l = \frac{(E_g/E_m)-1}{(E_g/E_m)+\xi} \quad (3)$$

$$\eta_t = \frac{(E_g/E_m)-1}{(E_g/E_m)+2} \quad (4)$$

$$E_m = w_pE_p + w_{pl}E_{pl} \quad (5)$$

$$\xi = 2\left(\frac{(w+l)/2}{t}\right) \quad (6)$$

where E_g and E_m represent the Young's modulus of the graphene and the polymer matrix, and E_p and E_{pl} are the Young's modulus of the PP and PP latex, respectively assuming that E_m has a linear addition relationship with E_p and E_{pl}, as written in Eq. (5). ν_g is the volume fraction of graphene. w_p and w_{pl} are the mass fraction of PP and PP latex, respectively. Since the parameter ξ depends on the geometry and boundary conditions of the effective fiber [48], the ξ

can be expressed as Eq. (6), where l, w, and t represent the average graphene sheets length, width, and thickness. The Young's modulus (E) of the chemically reduced graphene sheet, PP matrix, and PP latex is around 0.25 TPa [34], 1.02 GPa, and 0.05 GPa (also determined by tensile test), respectively, and their corresponding density (ρ) is 2.2 g/cm^3, 0.9 g/cm^3, and 0.93 g/cm^3. The statistical average value of l, w, and t is 1.0 μm, 0.7 μm, and 0.75 nm, respectively, as determined by AFM and TEM observations. According to Eqs. (1)–(5), two kind of predicted Young's modulus can be calculated under two hypotheses, namely graphene randomly distributed as 3D network throughout the polymer matrix, and graphene sheets aligned parallel to the surface of sample film [21,22]. As shown in Fig. 4B, as the graphene loading not exceeding 2.0 wt%, the experimental modulus agrees well with the theoretical simulation for the hypotheses that graphene sheets are aligned parallel to the surface of nanocomposite, indicating tensile load can be effectively transferred from the polymer matrix to graphene nanosheets. However, as shown in Table 2 and Fig. 4B, with further increasing graphene loading, the Young's modulus gradually approaches the theoretical simulation for the random dispersion of graphene sheets. This change, on one hand, can be attributed to the so-called critical point [22], e.g. 1.0 wt% (0.42 vol%) for our systems, and on the other hand, to the plasticization effect of PP latex still remains, even its modulus is taken into account. What's more, the statistical errors of graphene size are also responsible for the modulus change.

To investigate the potential effect of PP latex including plasticization, the tensile measurements of PP/PP latex blends with various PP latex contents were performed. The typical stress–strain curves of PP/PP latex blends are shown in Fig. 5C, it is clear that the presence of PP latex causes the reduction in all mechanical parameters. For instance, 4 wt% PP latex leads to a reduction by ~20%, ~50%, and 60% for tensile strength, Young's modulus and elongation at break, respectively, relative to neat PP. The reduction in the tensile strength and Young's modulus is primarily attributed to low strength and modulus of PP latex, as well as the small molecule surfactants and other additives, namely their plasticization effects. In the case of the elongation at break, the polar surfactant and additives in PP latex are mainly responsible for the decrease in the elongation. Because the amount of them will double with increasing graphene loading, their adverse impacts on the mechanical properties of composites will be much larger.

To clarify the reinforcement mechanism and load transfer from the polymer matrix to the filler, SEM images are employed to observe the micro-morphology of fracture surface of tensile sample. As shown in Fig. 6, section A and section B are, respectively, the fracture cross-section and side face of the nanocomposite with 1.0 wt% graphene after tensile measurement. For the fracture cross-section, SEM-A image clearly indicates that most of graphene are well-dispersed in the PP matrix (marked by white arrows), and SEM-A1/A2 images (the magnification of parts in SEM-A) show that the majority of graphene nanoplatelets are coated by PP latex (marked by black arrows), and some few-layers can also be observed. Upon drawing, the tough PP matrix will generally be oriented first along the tension direction, and then the crazing will evolve in the vicinity of weak interfaces until the material is

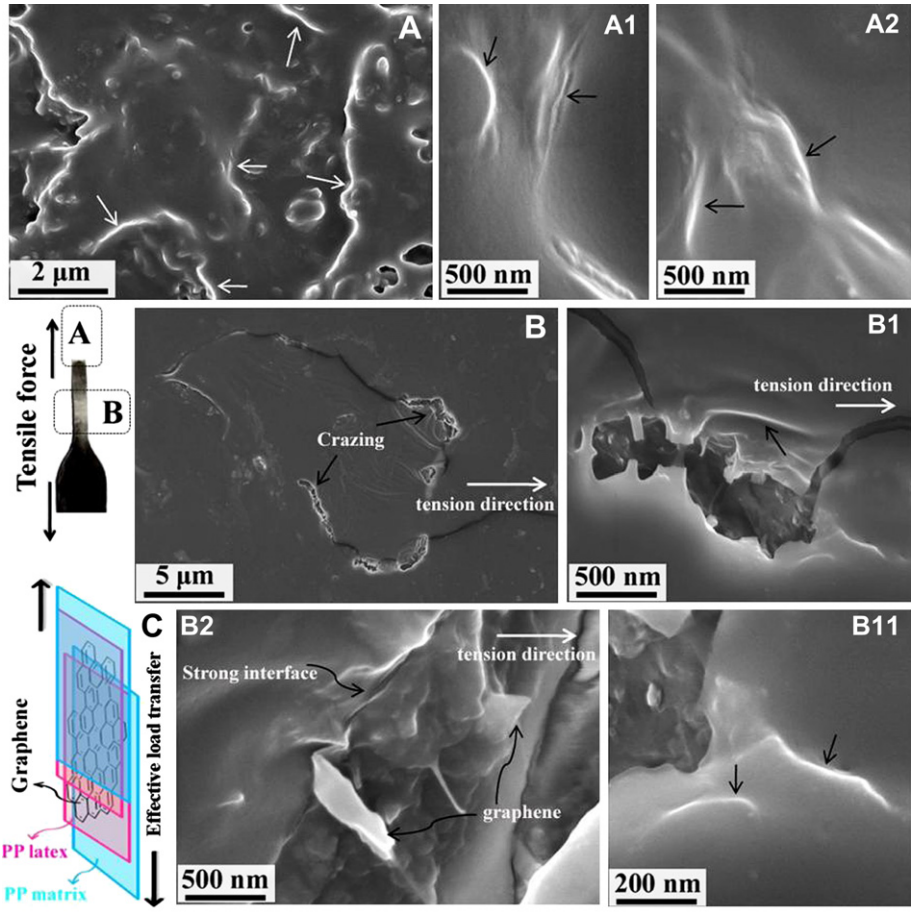

Fig. 6. (A) SEM cross-section images of the nanocomposite with graphene loading of 1.0 wt% after tensile test, (A1, A2) sectional magnification in A, and the arrows point to the graphene nanoplatelets; (B) SEM profile of the composite with graphene loading of 1.0 wt% after tensile test, (B1, B2) sectional magnification in B, (B11) sectional magnification in B1, and the black and white arrows point to the graphene sheets and tension direction; (C) Schematic representation of the structure of graphene/PP latex/PP matrix.

completely destroyed. SEM-B image clearly shows the evolution of crazing along the tension direction on the side face of tensile sample. SEM-B1/B11 images (the magnification of parts in SEM-B) indicate that the protruding graphene sheets coated by PP which are parallel to the tensile surface. Furthermore, SEM-B2 can more clearly display that the strong interfaces exist between graphene sheets and the polymer matrix, and the tensile load is effectively transferred from the PP matrix to the graphene sheets from the protruding graphene sheets pointed by arrows in Fig. 6B2. On the basis of SEM observations, a schematic model of the structure and load transfer is proposed and presented in Fig. 6C. The PP-coated graphene can be uniformly dispersed in PP matrix, and the tensile load can be effectively transferred from the PP matrix to the PP latex and then to graphene nanosheets due to strong interfacial adhesion among them. However, with increasing graphene loading, the plasticization effect of PP latex gradually overwhelms the reinforcement effect of graphene sheets, thus the mechanical performance starts to decrease.

3.3. Thermal properties of PP/graphene nanocomposites

Due to its characteristic of sheet structure analogous to layered silicates, graphene sheets will affect the dynamic of polymer chains and the thermal properties to some extent. Fig. 7 presents the storage modulus and loss factor plots as a function of temperature. As shown in Fig. 7A, the storage moduli of PP nanocomposites increase with increasing graphene loading below 1.0 wt% loading of graphene, while further increasing loading of graphene leads to a slight reduction in the modulus in the whole range of temperature. This trend agrees well with that of Young's modulus due to the plasticization effect of low modulus of PP latex. As the graphene loading is 1.0 wt%, the storage modulus reaches the maximum value (ca. 1.63 GPa) which is ~36% higher than that of neat PP (1.2 GPa). The magnitude of increase of storage modulus is lower than that of Young's modulus, which may be due to the difference of the measurement modes and the resolution of instruments. The glass transition temperature (T_g) is widely determined by the tan δ peak temperature in DMA [14,49,50]. As shown in Fig. 7B, there is a slight increase in T_g (ca. 2.5 °C) at 0.041 vol% (0.1 wt%) of graphene than that of neat PP, indicating the movements of polymer chain are restricted to certain degree. However, the magnitude of increment gradually reduces with increasing graphene loading, with only a 2.5% increment of T_g observed for the nanocomposites with 2.1 vol % (5.0 wt%) of graphene. The results can also be explained by the plasticization effect of PP latex. At a low graphene loading of 0.1 wt %, the mass fraction of PP latex was only 0.2 wt%, its plasticization can be ignorable relative to the restriction of graphene to the polymer chains. With increasing graphene loading, the content of PP latex doubles, as a result, the increment of T_g gradually reduces.

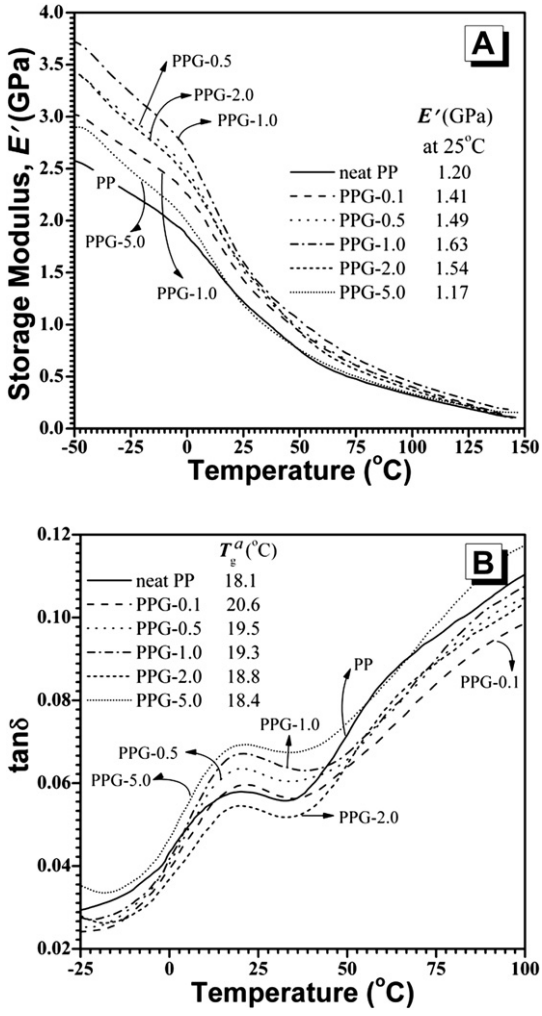

Fig. 7. (A) Storage modulus and (B) loss factor of PP/graphene nanocomposites with various graphene volume fractions. ^aT_g: glass transition temperature, which was determined from the temperature of tan δ peaks obtained from DMA tests.

Suspended graphene was reported to have a very high thermal conductivity of ca. 5000 W/m K [51], while neat PP is of low thermal conductivity about 0.2 W/m K [52]. Thus, to investigate the effect of the presence of graphene on the thermal conductivity of PP, the thermal conductivity neat PP and its graphene nanocomposites were performed and the results are shown in Fig. 8. As expected, the presence of graphene can significantly enhance the thermal conductivity of PP, and the conductivity monotonously increases with increasing graphene loading. For example, a loading of 5.0 wt% (2.1 vol%) graphene results in a thermal conductivity of 0.396 W/m K, about 2 times of that of neat PP (0.201 W/m K). Kalaitzidou et al. [52] incorporated 3.0 vol% exfoliated graphite nanoplatelets into PP and also obtained a close value of ~0.4 W/m K, relative to ~0.2 W/m K of neat PP. Additionally, the graphene obtained by chemical reduction of graphene oxide is rather defective, which will adversely affect the improvement of thermal conductivity of PP.

The thermal behaviors of pristine graphite and its derivatives, as well as dried PP latex in air are presented in Fig. 9. It is clear that pristine graphite is very thermally stable, only 4.8 wt% mass loss

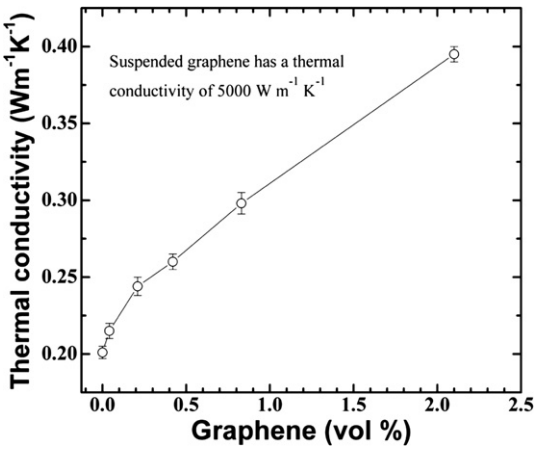

Fig. 8. Thermal conductivity of PP and its nanocomposites as a function of graphene loading.

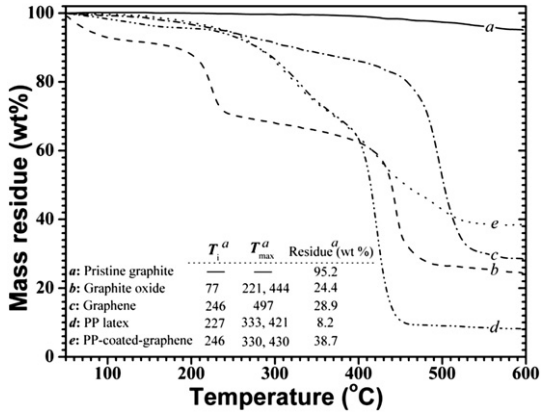

Fig. 9. TGA curves of graphite, graphite oxide, graphene, PP latex and PP-coated graphene in air condition. ^aT_i and $^aT_{max}$ represent the initial degradation temperature where 5 wt% mass loss occurs, and the maximum mass loss temperature where maximum loss rate takes place; the mass residue is obtained at 600 °C.

occurs upon heating to 600 °C. After oxidation, it starts to degrade from 77 °C, indicating the loss of some unstable oxygen containing oxygen groups or the absorbed water. It experiences a two-step degradation and maximum weight loss takes place at 221 °C and 444 °C, respectively, leaving a char residue of 24.4 wt%. After reduction, graphene turns thermally stable relative to GO, and starts to degrade at 246 °C due to the presence of oxygen, and maximum weight loss occurs at 497 °C, leaving a char residue of 28.9 wt%, indicating the presence of oxygen containing groups and some other defects. For pure PP latex, it degrades from 227 °C due to the oxidation degradation, and is also subjected to a two-step degradation, but only leaving a residue of 8.2 wt% due to the presence of highly stable chemicals like sodium ions introduced by the fabrication of PP latex. For PP-coated graphene, the curve of its thermal degradation is near that of PP latex below 450 °C. However, it is unexpected that its residue (~38.7 wt%) is much higher than that of graphene, because its theoretical residue is 15.0 wt%. The increasing char residue may be due to the thermal protection of char residue from the PP latex on the surface of graphene, since the graphene was coated by the PP latex.

Several studies [20,21] have demonstrated that incorporation of graphene sheets can enhance the thermal stability of PVA to different degree under nitrogen atmosphere, while Jeong's studies [18,19] revealed that incorporating functionalized graphene sheets accelerated the thermal degradation of polyurethane (PU) under inert condition. Since the polymeric materials are commonly used under air condition, it is much more important to investigate the effect of graphene sheets on thermal oxidation stability of the polymeric materials. As shown in Fig. 10, compared to the PP matrix, both initial degradation temperature (T_i) and maximum mass loss temperature (T_{max}) are monotonously shifted up to higher temperatures with increasing graphene loading, inferring an significant improvement of the thermal oxidation stability of PP due to the barrier effects of its sheet structure like clay planets. Neat PP starts to degrade at 244 °C (T_i) and T_{max} occurs at about 347 °C. After incorporation of 0.1 wt% and 1.0 wt% graphene, T_i values are increased by 13 °C (257 °C) and by 26 °C (270 °C), respectively. Moreover, the T_{max} values are also enhanced by 5 °C for 0.1 wt% graphene and by 19 °C for 1.0 wt% graphene loading, respectively. Wakabayashi et al. [12] observed that addition of 0.8 wt% graphite enabled the T_i (5 wt% mass loss) of PP to be delayed by ~15 °C in nitrogen condition, without determining the effect of graphite on the thermal oxidative degradation of PP in this study. Whatever, graphene has a great potential to enhancing the thermal stability of PP in air condition.

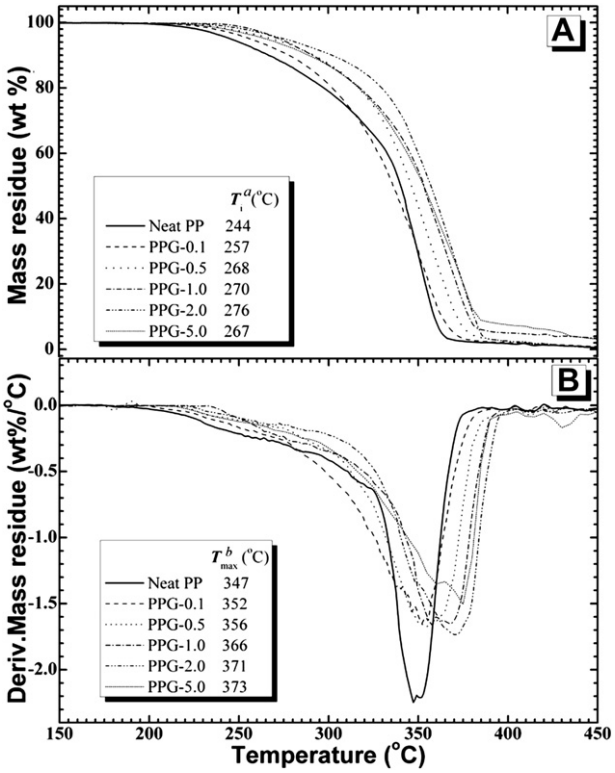

Fig. 10. (A) TGA and (B) DTG curves of PP/graphene nanocomposite with various graphene loadings, ^aT_i and $^bT_{max}$ represent the initial degradation temperature where 5 wt% mass loss occurs, and the maximum mass loss temperature where maximum loss rate takes place.

4. Conclusions

In summary, we have successfully fabricated the PP/graphene nanocomposites with well-dispersed exfoliated graphene nanosheets using an eco-friendly method, namely, first using latex technique and then via melt-blending technique. Considerable enhancement of the mechanical properties of PP is achieved by incorporating very low loading of graphene. The practical Young's modulus is consistent to that predicted by the Halpin–Tsai model at relatively low graphene loading, and the majority of graphene sheets are aligned parallel to the surface of nanocomposite. The experimental modulus deviates the predicted value at high loading of graphene because of the plasticization effect of low molecular weight PP latex overwhelming the reinforcement effect of graphene sheets. The external tensile load can be effectively transferred from the polymer matrix to graphene nanosheets through effective interfacial phase. The presence of graphene sheets to some extent restricts the movement or relaxation of the polymer chains, as evidenced by increased glass transition temperature. The thermal oxidative stability of PP is significantly improved by the addition of graphene sheets due to the barrier effect of lamellar structure. Though the mechanical properties of PP are improved remarkably, it still has the place to enhance the reinforcement effect of graphene sheets, and much work remains to be done, for example, how to choose and optimize the amount of the interfacial compatibilizer. Whatever, we provide an eco-friendly and effective strategy for fabricating high-performance graphene-based PP nanocomposites.

Acknowledgments

The authors would like to acknowledge the financial support from State 863 projects (No. 2010AA101704), Natural Science

Foundation of Zhejiang Province of China (No. Y3100124) and Scientific Research Foundation of Zhejiang Agriculture & Forestry University (No. 2351001088).

References

[1] Potts JR, Dreyer DR, Bielawski CW, Ruoff RS. Polymer 2011;52:5.
[2] Reichert P, Nitz H, Klinke S, Brandsch R, Thomann R, Mülhaupt R. Adv Funct Mater 2000;275:8.
[3] Zanetti M, Camino G, Reichert P, Mülhaupt R. Marcomol Rapid Commun 2000; 22:176.
[4] Ajayan PM, Schadler LS, Giannaris C, Rubio A. Adv Mater 2000;12:750.
[5] Thostenson ET, Ren ZF, Chou TW. Compos Sci Technol 2001;61:1899.
[6] Zheng W, Wong SC. Compos Sci Technol 2003;63:225.
[7] Zhou W, Lu XH, Wong SC. J Appl Polym Sci 2004;91:2781.
[8] Kalaitzidou K, Fukushima H, Drazl LT. Composites A 2007;38:1675.
[9] McAllister MJ, Li JL, Adamson DH, Schniepp HC, Herrera-Alonso AA, Milius DL, et al. Chem Mater 2007;19:4396.
[10] Alzari V, Mariani A, Monticelli O, Valentini L, Nuvoli D, Piccinini M, et al. J Polym Sci A Polym Chem 2010;48:5375.
[11] Lee CG, Wei XD, Kysar JW, Hone J. Science 2008;321:385.
[12] Wakabayashi K, Pierre C, Dikin DA, Ruoff RS, Ramanathan T, Brinson LC, et al. Macromolecules 2008;41:1905.
[13] Huang YJ, Qin YW, Zhou Y, Niu H, Yu ZZ, Dong Y. Chem Mater 2010;22:4096.
[14] Ramanathan T, Abdala AA, Stankovich S, Dikin DA, Herrera-alonso M, Pinter RD, et al. Nat Nanotechnol 2008;3:327.
[15] Kim H, Macosko CW. Macromolecules 2008;41:3317.
[16] Debelak B, Lafdi K. Carbon 2007;45:1727.
[17] Rafiee MA, Rafiee J, Wang Z, Song HH, Yu ZZ, Koratkar N. ACS Nano 2009;3: 3884.
[18] Raghu AV, Lee YR, Jeong HM, Shin CM. Macromol Chem Phys 2008;209:2487.
[19] Lee YR, Raghu AV, Jeong HM, Kim BK. Macromol Chem Phys 2009;210:1247.
[20] Xu YX, Hong WJ, Bai H, Li C, Shi GQ. Carbon 2009;47:3538.
[21] Liang JJ, Huang Y, Zhang L, Wang Y, Ma YF, Guo TY, et al. Adv Funct Mater 2009;19:2297.
[22] Zhao X, Zhang QH, Chen DJ. Macromolecules 2010;43:2357.
[23] Stankovich S, Dikin DA, Dommett GHB, Kohlhass KM, Zimney EJ, Stach EA, et al. Nature 2006;442:282.
[24] Fim FDeC, Guterres JM, Basso NRS, Galland GB. J Polym Sci A Polym Chem 2010;48:692.
[25] Lin Y, Jin J, Song M. J Mater Chem 2011;21:3455.
[26] Kim H, Kobayashi S, AbdurRahim MA, Zhang MJ, Khusainova A, Hillmyer MA, et al. Polymer 2011;52:1837.
[27] Wakabayashi K, Brunner PJ, Masuda JI, Hewlett SA, Torkelson JM. Polymer 2010;51:5525.
[28] Regev O, ElKati PNB, Loos J, Koning CE. Adv Mater 2004;16:248.
[29] Grossiord N, Loos J, Koning CE. J Mater Chem 2005;15:2349.
[30] Miltner HE, Grossiord N, Lu KB, Loos J, Koning CE, Mele BV. Macromolecules 2008;41:5753.
[31] Tkalya E, Ghislandi M, Alekseev A, Koning C, Loos J. J Mater Chem 2010;20: 3035.
[32] Hummers WS, Offeman RE. J Am Chem Soc 1958;80:1339.
[33] Stankovich S, Dikin DA, Pinter RD, Kohlhaas KA, Kleinhammes A, Jia Y, et al. Carbon 2007;45:1558.
[34] Gomez-Navarro C, Burghard M, Kern K. Nano Lett 2008;8:2045.
[35] Zhang HB, Zheng WG, Yan Q, Yang Y, Wang JW, Lu ZH, et al. Polymer 2010;51: 1191.
[36] Bose S, Kuila T, Uddin ME, Kim NH, Lau AKT, Lee JH. Polymer 2010;51:5921.
[37] Dresselhaus MS, Dresselhaus G, Jorio A, Souza Filho AG, Saito R. Carbon 2002; 40:2043.
[38] Tuinstra F, Koenig JL. J Chem Phys 1970;53:1126.
[39] Kudin KN, Ozbas B, Schniepp HC, Prud'humme RK, Aksay IA, Car R. Nano Lett 2008;8:36.
[40] Paredes JI, Villar-Rodil S, Solis-Fernandez P, Martinez-Alonso A, Tascon JMD. Langmuir 2009;25:5957.
[41] Liu MX, Guo BC, Du ML, Chen F, Jia DM. Polymer 2009;50:3022.
[42] Lonkar SP, Morlat-Therias S, Caperaa N, Leroux F, Gardeete JL, Singh RP. Polymer 2009;50:1505.
[43] Thompson A, Bianchi O, Amorim CLG, Lemos C, Teixeira SR, Samios D, et al. Polymer 2011;52:1037.
[44] Lin Y, Friedrich K. Compos Sci Technol 1993;46:187.
[45] Zhang QH, Fang F, Zhao X, Li YZ, Zhu MF, Chen DJ. J Phys Chem B 2008;112: 12606.
[46] Halpin JC, Kardos JL. Polym Eng Sci 1976;16:344.
[47] Schaefer DW, Justice RS. Macromolecules 2007;40:8501.
[48] Halpin JC, Thomas R. J Compos Mater 1968;2:488.
[49] Layek RK, Samanta S, Chatterjee DP, Nandi AK. Polymer 2010;51:5846.
[50] Zaman I, Phan TT, Kuan HC, Meng QS, La LTB, Luong L, et al. Polymer 2011;52: 1603.
[51] Prasher R. Science 2010;328:185.
[52] Kalaitzidou K, Fukushima H, Drzal LT. Carbon 2007;45:1446.